

Investigation of SiC Single Crystal Polishing by Combination of Anodic Oxidation and Mechanical Polishing

Xincheng Yin*, Shujuan Li*, Peng Chai

School of Mechanical and Precision Instrument Engineering, Xi'an University of Technology, Xi'an 710048, Shaanxi, China.

*E-mail: albertyinx@163.com (X. Yin), shujuanli@xaut.edu.cn (S. Li)

Received: 3 January 2020 / Accepted: 27 February 2020 / Published: 10 April 2020

For high-quality and effective polishing of SiC, a novel polishing technique that combines anodic oxidation and mechanical polishing (AOMP) is proposed herein. To clarify the SiC surface anodic oxidation mechanism, AOMP experiments were conducted. The results show that as a result of surface oxidation, the main elements of the modified surface were Si and O by X-ray diffraction (XRD), indicating that the SiC surface was modified and formed a SiO₂ oxide layer. Micro Vickers hardness tests revealed that the hardness of the modified surface greatly decreased to 1/9 of that of the as-received surface, which was easy to remove. Considering the experimental results, an anodic oxidation process model is proposed herein based on the inner-outer double-directional diffusion theory. During the oxidation process, a transition layer containing silicon oxycarbide (Si-C-O) was formed between the SiO₂ and SiC, the amount of which varied with the thickness of the oxide. Based on the Deal-Grove model, the relationship between the oxide layer thickness and oxidation time was determined, and the initial oxidation rate was 44.81 nm/min. The surface roughness after chemical mechanical polishing (CMP) was determined for different oxidation time and polishing time, and it was clear that when the anodic plasma oxidation rate matched the CMP rate, a just-polished surface was obtained.

Keywords: SiC single crystal; anodic oxidation; mechanical polishing; mechanism

1. INTRODUCTION

SiC is a promising next-generation semiconductor owing to its excellent physical and chemical properties such as a wide band gap, a high breakdown electric field strength, a high electron mobility, and good thermal conductivity; therefore it has widespread applications in high-power, high-efficiency and high-temperature fields such as the information industry and electronic devices [1]. To realize its excellent properties and performance in precision equipment and power devices, a smooth planarized surface without scratches or subsurface damage is essential. However, SiC is hard to polish by

conventional methods due to its high hardness and remarkable chemical inertness. During the SiC fabrication process, which involves crystal growth, slicing, lapping, etching, polishing and packaging, polishing is one of the key steps, as the surface roughness greatly affects device performance. Due to the high integration of computer chips, the wafer substrates are increasing in size and decreasing in thickness, which brings additional challenges to wafer polishing processes.

Currently, a variety of polishing techniques have been proposed as surface treatment methods for SiC. Mechanical polishing (MP) [2], as a conventional polishing method, has a high material removal rate (MRR), but a large number of scratches on the wafer surface and substantial subsurface damage inevitably occur due to the use of hard abrasives, thus damaging the surface integrity [3], and making mechanically polished wafers unacceptable for certain applications. Hydrogen etching polishing [4] has been adopted to etch the SiC wafers; however, the surface smoothness is difficult to control, and the surface quality is poor due to the randomness of the etched surface and uneven erosion amount. Also, chemically combined fluorine still remains on the surface, and other procedures may be needed to remove the fluorine. Chemical mechanical polishing (CMP) [5], which combines chemical etching and mechanical polishing, has widespread applications in finishing planarization processes. However, it is difficult to avoid the appearance of certain major defects such as micropipes and planars on the surface of polished SiC wafer [6]; CMP has a high cost because of the use of slurries and other chemicals. Plasma-assisted polishing (PAP) [7-9], which combines surface modification via atmospheric-pressure plasma irradiation and soft abrasive polishing of the modified layer, has complex facility requirements and may cause environmental pollution. Electrochemical mechanical polishing (ECMP) [10-13] oxidizes the surface first and then removes the modified layer by mechanical polishing; however, etch pits are easily generated on the polished surface, increasing the surface roughness.

To resolve these problems and obtain a scratch-free, pit-free and atomically flat surface with a high efficiency, a novel approach that combines surface modification and mechanical polishing, named anodic oxidation and mechanical polishing (AOMP), has been proposed. The ion energy in the plasma is approximately several electron volts, which can avoid mechanical damage to the SiC surface by ion bombardment during the plasma exposure period [14]. In this technique, the oxidation of the reactive plasma modifies the SiC surface to form a soft layer; simultaneously, the modified layer is removed by soft abrasive polishing. AOMP is an environmentally friendly polishing technique owing to the use of a green slurry material, and it can also be applied to polish other brittle and hard-to-machine materials, such as SiC, GaN and sapphire.

This paper proposes an AOMP approach for SiC polishing and AOMP experiments were conducted. SiC surface anodizing and abrasive polishing characteristics are reported herein. The surface of the as-received SiC wafer was oxidized and formed a SiO₂-modified layer that was easy to remove. On the basis of the inner-outer double-directional diffusion theory, a model for the SiC plasma anodic oxidation process was built to explain the material removal mechanism during the AOMP process. By comparing the surface roughness before and after oxidation with SWLI, we obtained the relationship between the oxide layer thickness and oxidation time, and a just-polished surface formed when the anodic plasma oxidation rate matched the CMP rate.

2. EXPERIMENTAL METHODS

2.1 AOMP concept

AOMP contains two steps: anodic oxidation, which modifies the surface, and abrasive polishing, which removes the modified layer with a mechanical polishing process. Fig. 1 shows the two steps contained in the AOMP process. Oxygen and the electrons generate an oxygen plasma (O^{2-}) which is a strong oxidizer, and as a result, SiC is oxidized and transforms into silicon dioxide (SiO_2), which becomes the modified layer. Since cerium dioxide (CeO_2) abrasives are softer than SiC but harder than the modified layer, only the oxide layer is removed during the polishing process, and scratches and subsurface damage are not introduced.

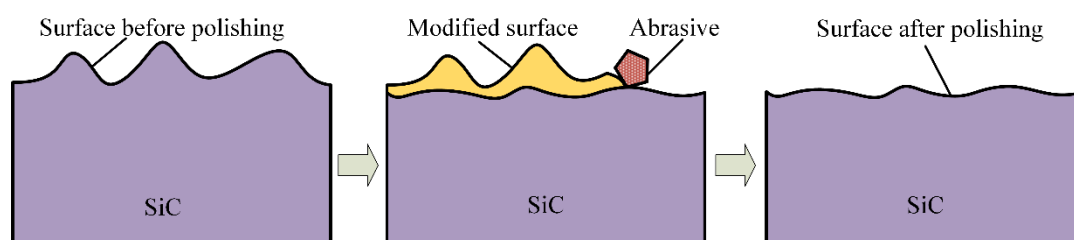


Figure 1. AOMP steps.

SiC single crystal has high hardness (Mohs hardness 9.5), and the hardness of SiO_2 (Mohs hardness 7.0) is much lower than that of SiC. Through a chemical modification approach, a surface layer on the SiC can be modified to form a SiO_2 thin film that can be removed by soft CeO_2 (Mohs hardness 6) abrasive particles. After the SiO_2 is removed by the CeO_2 abrasive particles, a fresh SiC surface is exposed and a new round of corrosion begins. At the same time, due to the preferential corrosion and removal mechanism of the surface bumps, a cyclic process of oxidation-modification to mechanical-removal to reoxidation-modification occurs, which results in a high material removal rate and decreased surface roughness. After several cycles of surface anodic oxidation and simultaneous abrasive polishing, a smooth surface is obtained.

2.1.1 Anodic oxidation of the SiC surface

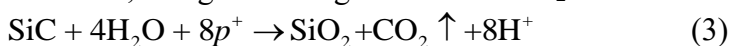
When the polishing solution is in contact with the SiC surface, H_2O molecules undergo a tribochemical reaction with the SiC surface to form a very small amount of SiO_2 , but the process is quite slow [15]:



In an energized state, the H_2O molecules in the polishing solution that receive an electron are dissociated into hydrogen ions (H^+) and the hydroxide ions (OH^-) by ionization:

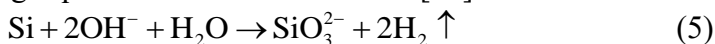


The electrochemical etching of SiC involves the SiC surface oxidation and partial dissolution of the formed oxide, along with the generation of CO_2 and CO bubbles. The reaction is as follows [16]:





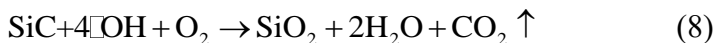
The chemical properties of the SiC single crystal are stable, but the dangling bonds of Si atoms on the SiC (0001) surface (Si-face) are unstable; thus the Si atoms can react with the OH⁻ in the polishing liquid due to the high temperature and high pressure conditions at the friction interface between the polishing liquid and the wafer interface [17]:



At the moment of electrification, a dense oxygen film is rapidly generated on the SiC surface, then the oxygen is dissociated into O²⁻, which has oxidation properties, by the plasma discharge, and the active and excited Si atoms on the Si-face are oxidized to SiO₂:



Since the oxidation potential of hydroxyl radicals (•OH) (2.80 V) is greater than that of oxygen (2.42 V), the oxidation ability of •OH is higher than that of oxygen radicals. Thus •OH with strong oxidation oxidizes the surface of the SiC to form a SiO₂-modified layer with a hardness that is much lower than that of SiC, and the generated CO diffuses outward [18]. The generated SiO₂ then reacts with OH⁻ to form SiO₃²⁻, accelerating the dissolution of the SiO₂ in the slurry [19, 20]. The reaction equations are:



According to the above reactions, SiC reacts with O²⁻ and •OH to form a soft SiO₂-modified layer, which is easy to remove by soft abrasive particles.

2.1.2 Abrasive polishing of the modified layer

When the anodic oxidation reaction occurs on the SiC surface, the generated soft oxide layer is easily removed during CMP process. The CMP model is shown in Fig. 2. During the polishing process of the SiC wafer, the SiC single crystal surface to be polished is in close contact with the polishing pad, and the polishing solution containing CeO₂ enters into the tiny gap between the SiC wafer and the polishing pad. The surface of the wafer is in contact with the polishing pad, which moves at a high speed, and the heat generated by friction maintains the chemical reactions; meanwhile, the microscopic region where the wafer contacts the polishing pad is in a high-temperature and high-pressure state, which accelerates the chemical reaction rate at the bumps on the wafer surface. Due to friction, the kinetic energy of the CeO₂ abrasive particles impacts with, collides with and shears the modified layer to peel off. After the polishing solution washes the modified layer, a fresh surface is exposed to form a new reaction layer. This cycle finally achieves the purpose of reducing the roughness of the wafer surface and producing SiC planarization [21].

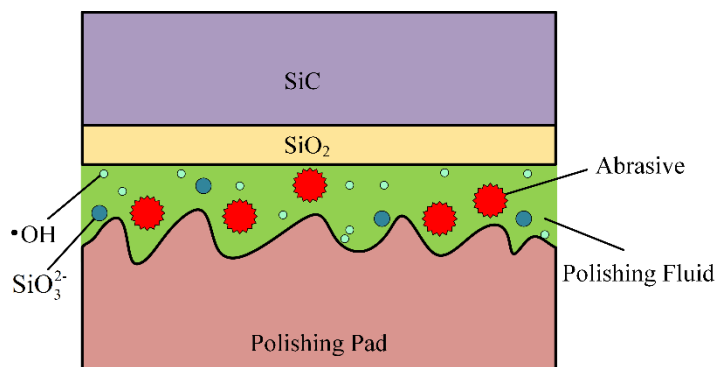


Figure 2. Chemical mechanical polishing model showing the modified layer.

During the CMP polishing of SiC, since the hardness of abrasive (CeO_2) is lower than that of SiC but higher than that of the modified layer (SiO_2), only the modified layer is removed, and surface scratches or subsurface damage are hardly introduced to the base material. Therefore, it is considered that the SiC surface can be polished without damage. During the whole AOMP process, plasma oxidation modifies the SiC surface and CeO_2 abrasive preferentially removes the soft modified layer. Since plasma oxidation and mechanical polishing are simultaneously performed, a scratch-free and damage-free SiC surface is obtained.

2.2 AOMP experimental

Schematic diagram of the AOMP experimental apparatus is shown in Fig. 3. The device consisted of two components that were used to investigate the principle removal mechanism: an anodic oxidation system and a mechanical polishing unit. The anodic oxidation system contained a pulse power supply, anode (4H-SiC specimen), cathode (stainless steel electrode), and electrolyte (polishing liquid). The mechanical polishing unit included a polishing pad, abrasive slurry, rotary table, and SiC polishing head.

The SiC wafer was fixed on the polishing head by a conductive adhesive, and the electrode holder was connected with the inner ring of the brush. The polishing head and the conductive brush outer ring connected with the positive electrode and the negative electrode of the pulse power supply, respectively. The polishing head was driven by a motor and rotated the SiC wafer, the back surface of the polishing pad was pasted to the upper surface of the rotating table, and the rotating table and the electrode holder were driven to rotate synchronously by the same motor. The rotary table had through-holes, in which the stainless steel electrodes can move up and down. The distance between the bottom surface of the SiC wafer and the top surface of the electrode was adjusted by the up and down movement of the inner ring of the brush. A stable plasma was generated by optimizing the moving speed of the rotary table and SiC polishing head. The nozzle sprayed a certain concentration of the polishing liquid at a proper flow rate, the wafer and the electrode were electrically connected by the polishing liquid, and the power supply provided a potential difference between the wafer and the electrode during processing. The surface of the SiC wafer was electrochemically oxidized by the plasma, and then the oxidized layer was removed by abrasive slurry during the mechanical polishing process. All experiments were conducted at room temperature.

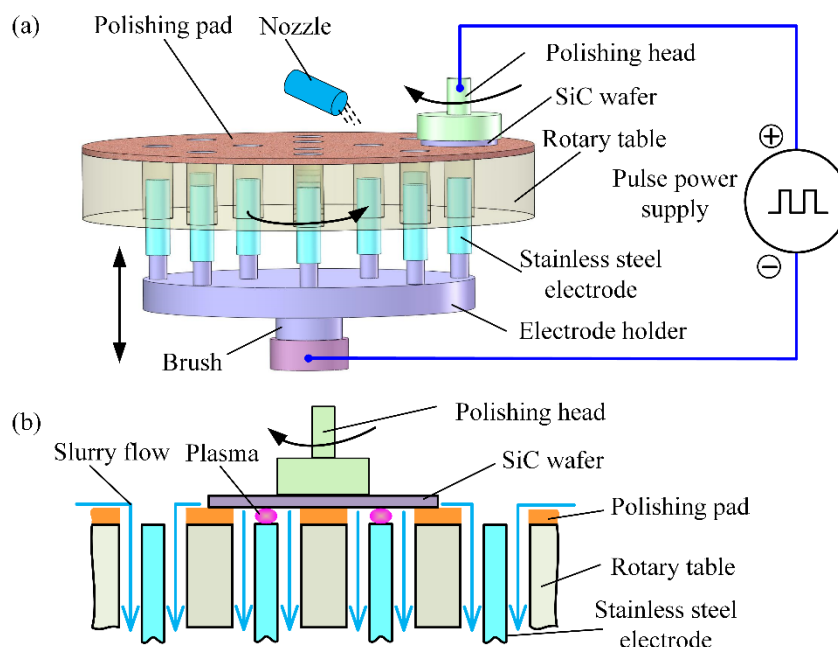
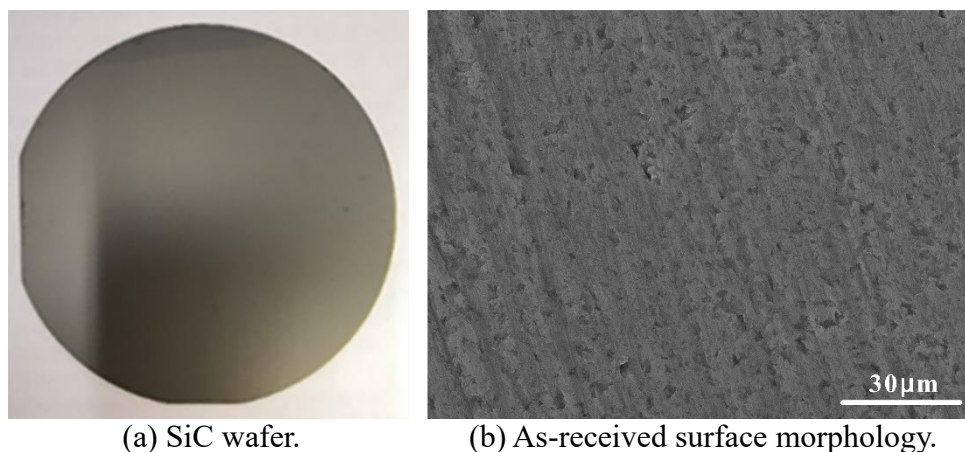


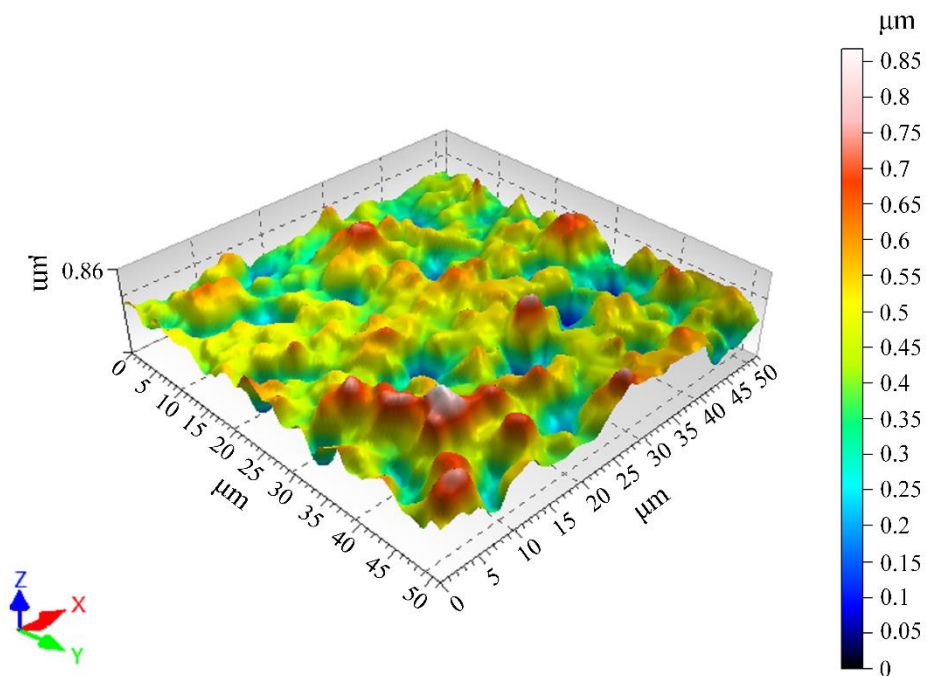
Figure 3. Schematic of the AOMP experiment: (a) apparatus and (b) polishing details.

The experiments adopted a commercially available 2-inch 4H-SiC wafer (on-axis, off-angle $\pm 0.5^\circ$, n-type) supplied by Hefei Crystal Technical Material Co. Ltd. Its thickness was 340 μm , and the resistivity was approximately 0.015 ~ 0.028 $\Omega\cdot\text{cm}$. The shape and surface morphology of the as-received SiC wafer is shown in Fig. 4. The anodic oxidation and abrasive polishing experiments were simultaneously conducted under the conditions noted in Table 1. All experiments were conducted on the Si-face ((0001) planar surface), which is the most widely used face. During the chemical-mechanical removal part, the SiC wafer was installed on the rotary table. The polishing temperature was 25°C and the polishing slurry contained 30% (wt) CeO_2 ($\phi 190\text{ nm}$) with a flow rate of 50-100 mL/min. Due to the high electrochemical activity of the chloride ion (Cl^-) in NaCl, it has a strong permeability during electrochemical reactions [22]. Adding NaCl to the electrolyte enhanced ion diffusion through the oxide layer and improved the oxidation process.



(a) SiC wafer.

(b) As-received surface morphology.



(c) As-received 3D surface morphology.

Figure 4. As-received SiC wafer and its surface morphology.

Table 1. Experimental conditions for the AOMP process.

Items	Values
Load (psi)	6.5
Voltage (V)	80
Frequency (kHz)	20
Duty cycle (%)	50
Electrolyte	Deionized water + NaCl 0.5%wt
Slurry	Water + CeO ₂ 30% wt
Polishing head rotation speed (rpm)	250
Rotary table rotation speed (rpm)	150
Anodic oxidation time (min)	5
Polishing time (min)	5

To facilitate the fixing of the SiC single wafer and adjust the surface roughness, the SiC wafers were pre-processed with double-sided grinding and mechanical polishing. Before the experiments, the sample surfaces were treated in a mixed solution with a 97 wt% H₂SO₄ and 34 wt% H₂O₂ (volume ratio of 4:1) for 10 min to remove contaminants and oxides, and then, the wafers were dipped in a concentrated HF solution (50 wt%) for 10 min. Finally, the sample was rinsed with deionized water for 10 min and blown dry in a pure stream of N₂ to avoid the influence of dissolved elements.

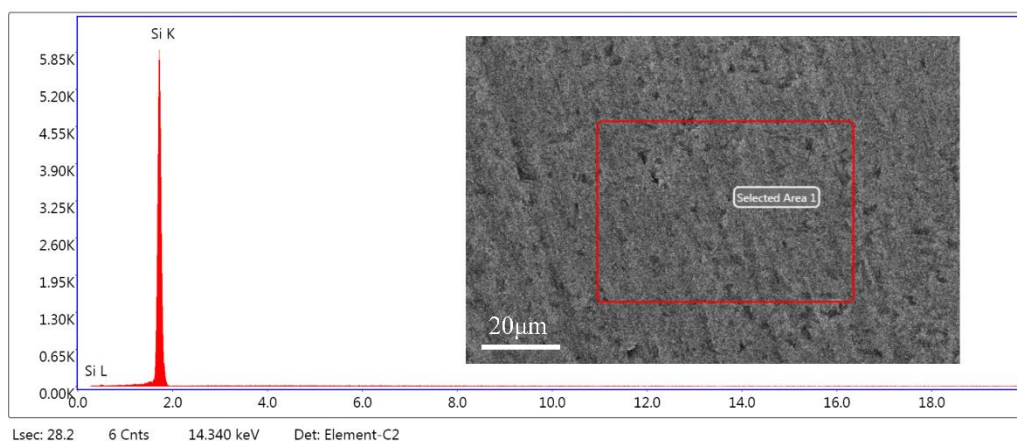
The surface morphology of the SiC substrate before and after AOMP was observed by scanning electron microscopy (SEM, TESCAN VEGA3). The substrate was analyzed with X-ray diffraction (XRD) (TESCAN VEGA3) to confirm its material composition. The hardness of the as-received SiC surface and that of the modified surface after plasma oxidation were examined by Micro Vickers hardness tests (Automatic Hardness testing system, Mitutoyo HM-200). The surface roughness before

and after ECMP was measured by scanning white light interferometer (SWLI, Leica DCM 3D).

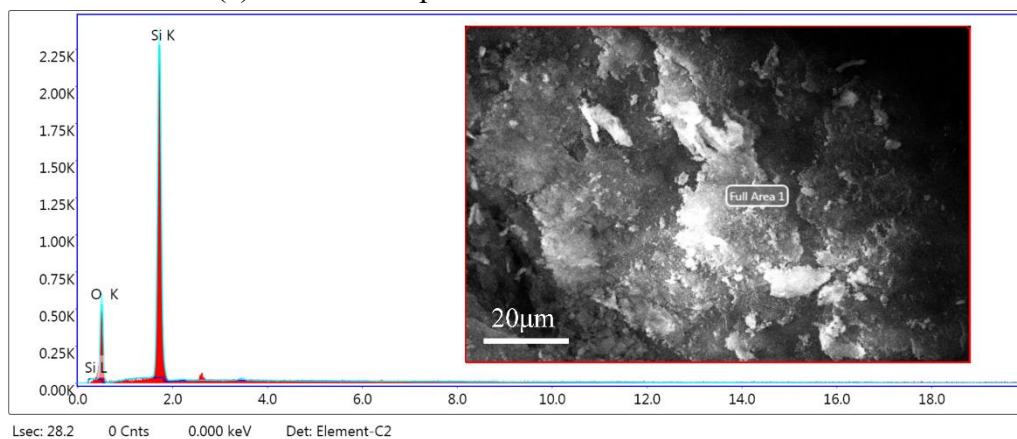
3. RESULTS AND DISCUSSION

3.1 Experimental results and analysis

The surface composition of as-received SiC and that of the modified surface by the anodic oxidation treatment was detected by XRD. Fig. 5 shows the surface composition before and after oxidation. In Fig. 5(b), after surface oxidation, the O element was obviously detected. The XRD results indicate that the main elements on the modified surface were Si and O, indicating that the surface of the as-received SiC wafer was oxidized and that a modified layer was formed.



(a) Surface composition of the as-received SiC.



(b) Surface composition of SiC after anodic oxidation.

Figure 5. Comparison of the components on the SiC surface before and after oxidation.

The energy spectrum of each element on the SiC surface after anodic oxidation treatment is shown in Fig. 6. The surface element composition after oxidation is shown in Table 2. This result indicates that the SiC surface was oxidized by the anodic oxidation treatment, resulting in a soft and easily removable SiO_2 modified layer and CO gas. Thus, there was a large increase in O and a significant decrease in C on the SiC surface.

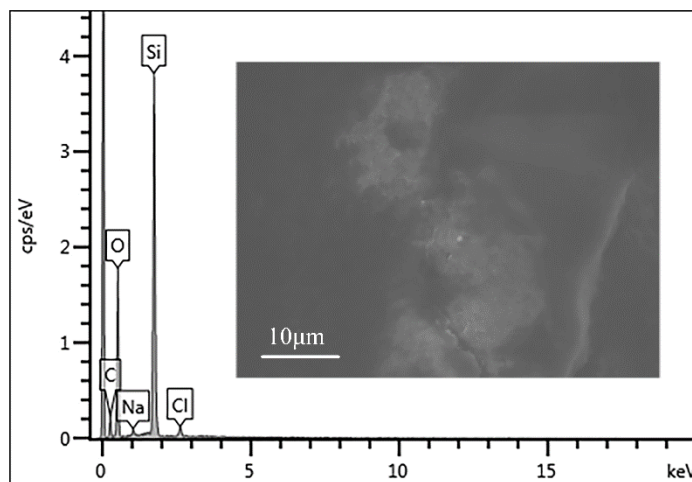


Figure 6. Energy spectrum of each element after oxidation.

Table 2. Surface composition after the oxidation process.

Element	wt%	wt% Sigma	Atomic percentage
C	21.84	1.25	30.89
O	47.94	0.95	50.89
Na	0.70	0.14	0.52
Si	28.40	0.60	17.18
Cl	1.11	0.11	0.53
Total	100.00	-	100.00

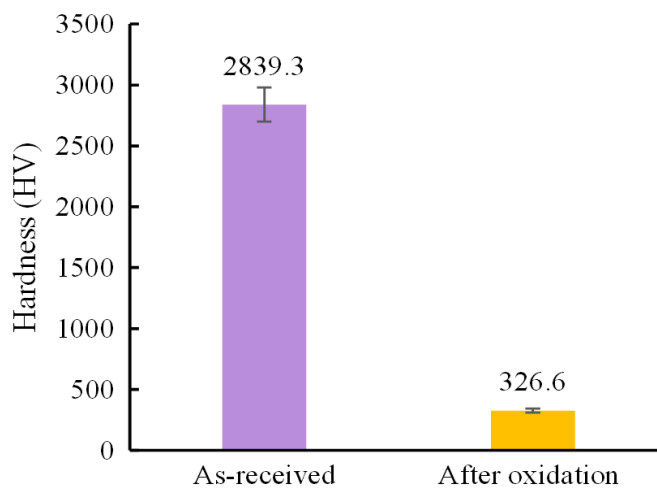


Figure 7. Surface hardness of SiC before and after oxidation.

To confirm that the hardness of the modified surface decreased, the hardness of the as-received SiC surface and that of the modified surface were examined by Micro Vickers hardness tests. As shown in Fig. 7, the hardness of the 4H-SiC surface decreased from 2839.3 HV to 326.6 HV after plasma oxidation. The surface hardness after oxidation was close to 1/9 that of the as-received SiC surface hardness, which is close to the ratio of the 4H-SiC surface hardness reductions from 37.4 ± 0.5 GPa to 4.5 ± 0.8 GPa before and after oxidation, respectively, in Reference [23]. Thus, the soft oxide layer was

easily removed during the polishing process, which improved the polishing efficiency.

Fig. 8 shows the SEM images of the SiC surface morphology after the plasma anodizing process. Irregular protuberances were generated, and cracks were distributed around the protuberances after the surface was oxidized. This might be because SiC has different a number and arrangement of Si atoms and C atoms in the different crystal directions in the crystalline material, resulting in anisotropy of SiC crystals. Thus, different crystal grains in SiC samples have different crystal lattice parameters. When the Si surface was oxidized, the expansion force caused the oxides of the initial SiC grains to squeeze each other due to the randomness of the direction of the expansion force; the protrusions were generated by the extrusion force, and cracks were formed by the expansion force produced by the subsurface oxidation. Fig. 9 shows the morphology of SiC oxidized surface after CMP. Since the hardness of the SiO₂ is significantly lower than that of the initial SiC sample, the protuberances and cracks on the soft oxide layer increase the contact area with the CeO₂ particles during the CMP process, which help improved the MRR and surface quality. Fig. 10 shows the SWLI image of the SiC surface after CMP processed, the surface roughness was Ra 1.54 nm after the measurement. This indicates that the oxide layer was merely removed and an ultra-smooth surface without scratches and pits was obtained.

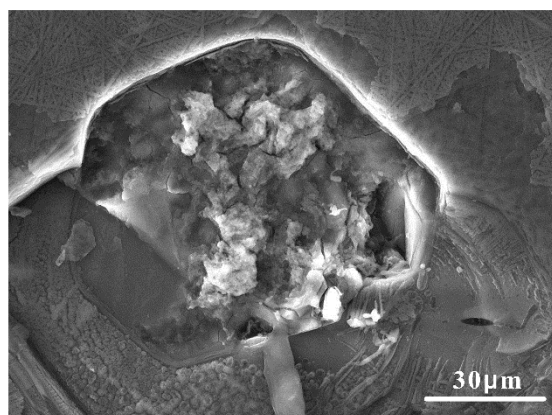


Figure 8. SiC surface after oxidation.

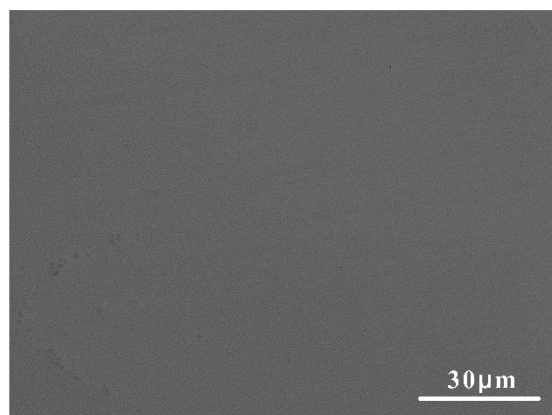


Figure 9. SiC oxidized surface after CMP.

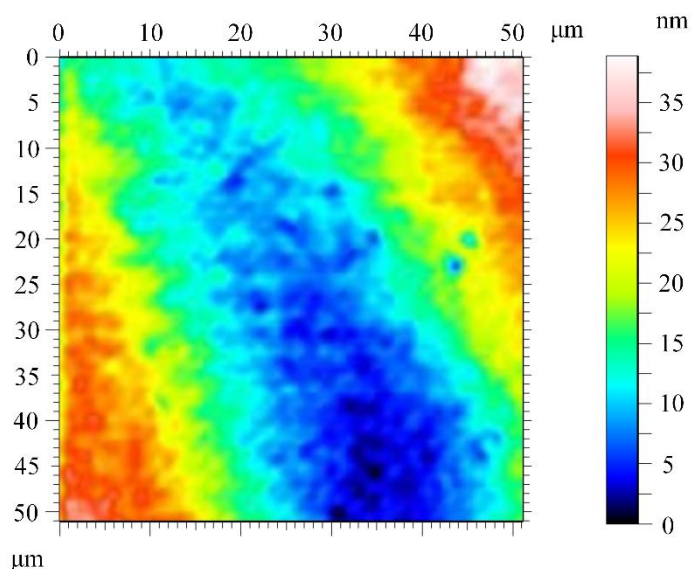


Figure 10. SWLI image of the SiC surface after CMP processing (Sz: 38.9 nm, Sa: 6.83 nm).

During the AOMP process, anodic oxidation of the SiC wafer surface and chemical abrasive mechanical polishing of the oxide layer are simultaneously carried out; that is, when the surface is oxidized, the generated oxide layer is immediately removed by CMP, which means that the plasma oxidation during the AOMP process is always maintained in the initial oxidation stage. Therefore, it can be considered that the MRR during AOMP is determined by the initial oxidation rate during plasma oxidation process.

3.2 Investigation of the plasma anodic oxidation mechanism

To investigate the plasma anodic oxidation mechanism during AOMP, an anodic oxidation process model is proposed based on the inner-outer double-directional diffusion theory. Fig. 11 shows a schematic of the double-directional diffusion during SiC plasma anodic oxidation. During the anodization process, H_2O in the electrolyte is ionized to generate hydroxyl radicals ($\bullet\text{OH}$) and a negative oxygen plasma (O^{2-}). With reference to the Deal-Grove model [24-26], according to the principle of inner-outer double-directional diffusion and the fact that the SiO_2 has micropores, high concentrations of the generated $\bullet\text{OH}$ and O^{2-} diffuse towards the electrode surface that has low concentrations of these species, the $\bullet\text{OH}$ and O^{2-} are gradually be transported from the gas phase layer to the outer surface of the oxide layer, and then diffuse inward through the SiO_2 oxide layer with a thickness of X_0 . When diffusing to the SiO_2 -SiC interface, they continue to react with the SiC, during which CO and H_2 gases are generated. When increasing concentrations of CO and H_2 accumulate to a certain extent, they begin to diffuse towards the direction with a lower concentration and away from the electrode surface and diffuse out through the oxide layer. Other accompanying reaction products such as H_2 escape from the oxidized surface and some reaction products such as C delaminate from the oxidized surface.

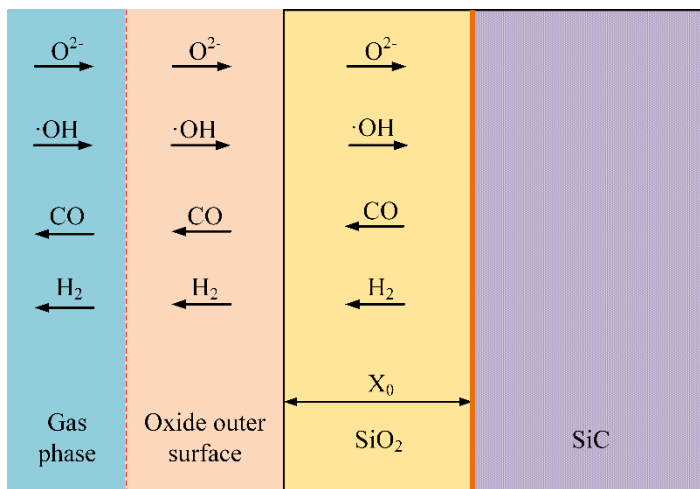


Figure 11. Schematic of double-directional diffusion during SiC anodic oxidation

Since the density of SiC (3.22 g/cm³) is greater than that of SiO₂ (2.23 g/cm³), the molar mass of SiC (40.096 g/mol) is less than that of SiO₂ (60.084 g/mol), and the number of Si atoms remains unchanged when SiC is oxidized to SiO₂, thus the volume of the oxide expands during the oxidation process [27]. Suppose that the thickness of SiC consumed during the oxidation process is X_{SiC}, the thickness of the generated SiO₂ oxide layer is X₀, and the bulk density of Si atoms in SiC and SiO₂ is N_{SiC} and N_{SiO₂} respectively. Then X_{SiC} can be expressed as:

$$X_{SiC} = X_0 \frac{N_{SiO_2}}{N_{SiC}} \tag{11}$$

According to the parameters in References [28-30], N_{SiC} = 4.82 × 10²²/cm³, N_{SiO₂} = 2.21 × 10²²/cm³, X_{SiC} = 0.458X₀, that is, to generate a SiO₂ oxide layer with a thickness of X₀, it takes approximately 0.458X₀ thick SiC layer. Due to adhesion with the SiC surface, the expansion of the oxide layer occurs mainly perpendicular to the interface [31]. A quantitative schematic diagram of the SiC anodic oxidation volume expansion process is shown in Fig. 12. A transition layer containing silicon oxycarbide (Si-C-O) is formed between the SiO₂ and SiC owing to the effect of oxidation, the amount of which varies with the thickness of the oxide [7].

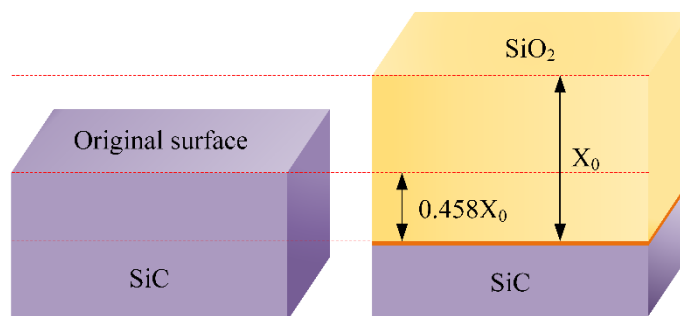


Figure 12. Quantitative schematic of the SiC anodizing volume expansion process

In the Deal-Grove model [24], the oxidation model for Si has the following relationship:

$$X^2 + AX = B(t + \tau) \tag{12}$$

where X is the thickness of the oxide layer, t is the oxidation time, τ is related to the initial thickness of the oxide on the Si surface, and the coefficient B and B/A are the parabolic rate constant and linear rate constant, respectively. If the growth rate of the oxide layer is linear, the reaction at the interface can be controlled by the rate; if the growth rate of the oxide layer is mainly a parabolic state relationship, oxygen diffusion through the oxide film is a rate controlling step.

Because the Deal-Grove model does not include the external diffusion of CO in the oxidation process of Si, it cannot be directly applied to the growth of SiC oxide layers [25], and the external diffusion factors need to be considered for an appropriate correction.

The anodic oxidation of SiC surface was analysed based on the principle of inner-outer double-directional diffusion, and a schematic of the plasma anodic oxidation process is shown in Fig. 13. Through the plasma ionization reaction, H_2O in the polishing solution is dissociated into $\bullet OH$ and O^{2-} , and then the two oxidants react with the SiC surface to form an oxide layer; the $\bullet OH$ and O^{2-} continuously diffuse through the oxide layer to the interface between the SiO_2 and SiC to participate in the next reaction. The gas products CO and H_2 diffuse outward through the oxide layer and overflow in the form of gas.

During the of SiC anodic oxidation process, the ions involved in the oxidation reaction are $\bullet OH$ and O^{2-} , and the spilling gas is CO and H_2 . In the equilibrium state, their concentrations in the electrolyte assumed to be $C_{O^{2-}}^E$, $C_{\bullet OH}^E$, C_{CO}^E and $C_{H_2}^E$. Their concentrations on the outer surface of the oxide layer are $C_{O^{2-}}$, $C_{\bullet OH}$, C_{CO} and C_{H_2} . Their transfer coefficients in the electrolyte are $h_{O^{2-}}$, $h_{\bullet OH}$, h_{CO} and h_{H_2} . Their diffusion coefficients in the formed oxide layer with a thickness of X_0 are $D_{O^{2-}}$, $D_{\bullet OH}$, D_{CO} and D_{H_2} . The forward and reverse reaction rate constants of the reaction are K_f and K_r , respectively.

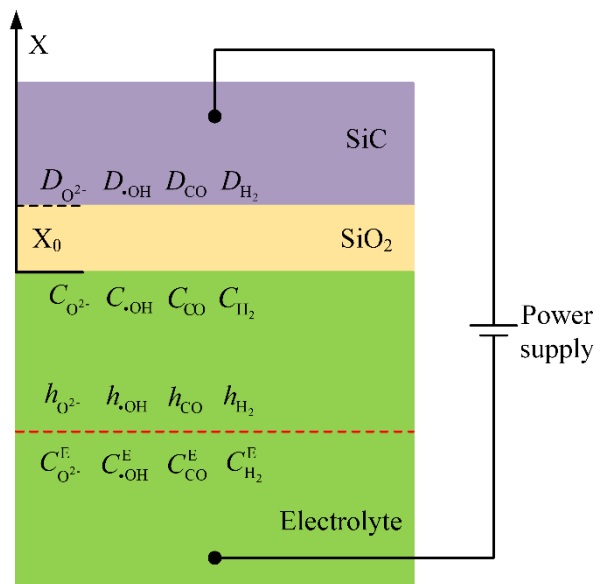


Figure 13. Schematic of the SiC anodizing process.

The oxidation reaction flux F is:

$$F = K_f C_{O^{2-}} + K_f C_{\bullet OH} - K_r C_{CO} - K_r C_{H_2} \tag{13}$$

When in an equilibrium state, the relationship between the oxidation reaction flux F and the

oxidation flux of each ion (molecule) is:

$$F : F_{O^{2-}} : F_{gOH} : F_{CO} : F_{H_2} = 1 : 1 : 4 : 1 : 2 \tag{14}$$

Referring to Eq. (12), the relationship between the oxide thickness X_0 and the oxidation time t is:

$$X_0^2 + AX_0 = B(t + \tau) \tag{15}$$

The number of oxidant molecules required to oxidize the SiC into a unit volume layer is set as N_0 , and the corresponding linear rate constant B and parabolic rate constant $\frac{B}{A}$ are:

$$\frac{B}{A} = \frac{(K_f C_{O^{2-}} + K_f C_{gOH} - K_r C_{CO} - K_r C_{H_2}) / N_0}{1 + \frac{4K_f}{h_{gOH}} + \frac{K_f}{h_{O^{2-}}} + \frac{K_r}{h_{CO}} + \frac{2K_r}{h_{H_2}}} \tag{16}$$

$$B = \frac{(K_f C_{O^{2-}} + K_f C_{gOH} - K_r C_{CO} - K_r C_{H_2}) / N_0}{\frac{K_f}{D_{O^{2-}}} + \frac{4K_f}{D_{gOH}} + \frac{K_r}{D_{CO}} + \frac{2K_r}{D_{H_2}}} \tag{17}$$

3.3 Calculation of oxidation thickness

During oxidation of the SiC surface, a modified layer is formed. To demonstrate the relationship between the oxide layer thickness and oxidation time during SiC anodic oxidation, the actual oxidant thickness can be calculated by SWLI scanning [32]. Since the oxidized layer can be etched by HF, the surface of the SiC single crystal before and after oxidation was detected by SWLI and compared, then the oxide layer thickness was calculated. The relationship between oxide layer thickness and time is shown in Fig. 14. It is found that the thickness of the oxide layer increased exponentially at the initial stage of oxidation owing to the porous structure of the oxide layer. Then, the growth rate of the oxide layer decreased due to the passivation reaction on the reaction surface, which increased the resistance of the oxide layer, thus the number of charged species passing through per unit time was reduced. The decreased anodic oxidation reaction rate decreased the formation rate of the oxide layer thickness.

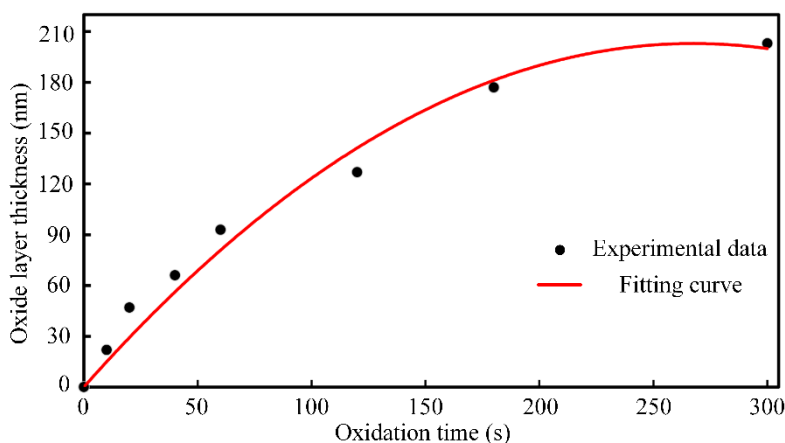


Figure 14. Variation of oxide layer thickness with time.

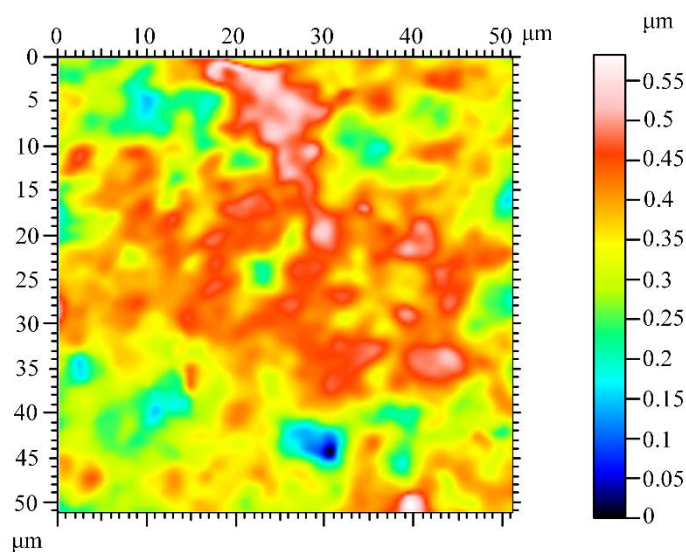
The relationship between the oxide layer thickness x (nm) and the oxidation time t (s) was obtained by fitting the calculated oxide layer thickness data according to the Deal-Grove model:

$$t = 0.0024x^2 + 1.339x \quad (18)$$

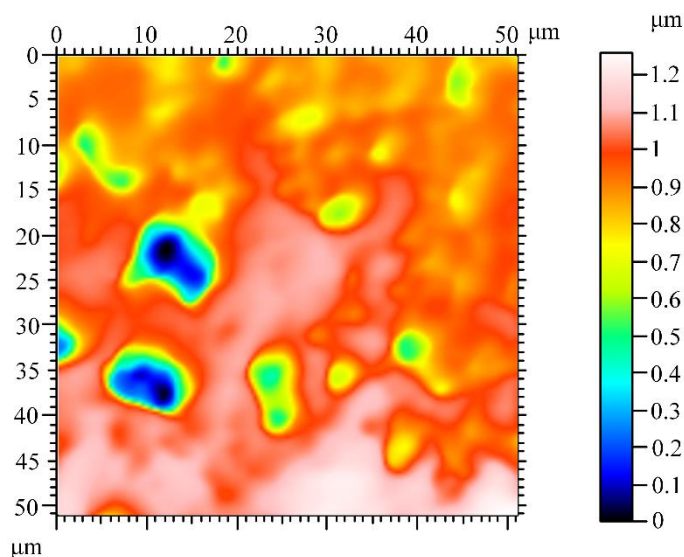
From Eq. (18), the SiC surface oxidation rate at the initial oxidation rate is 44.81 nm/min, thus it provided a sufficient thickness for continuous CMP polishing.

3.4 Surface roughness after CMP

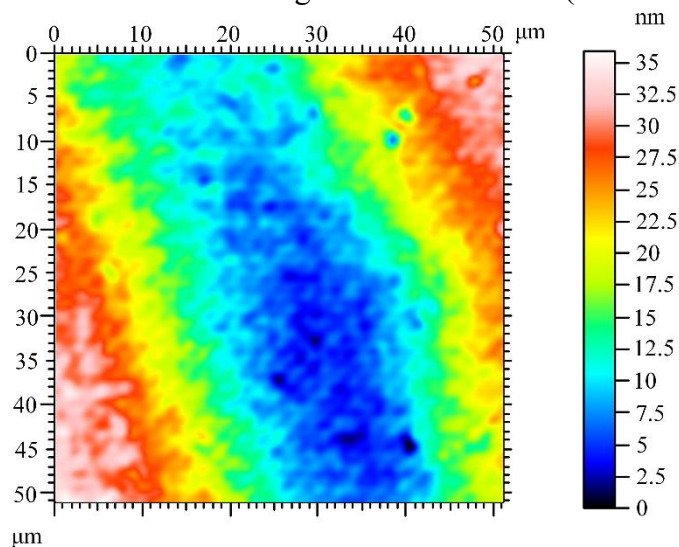
When a certain thickness of the SiO₂ oxide layer was formed, it was polished by the CeO₂ abrasive simultaneously. Fig. 15 shows the SWLI images of the SiC surface morphology and roughness under different oxidation times and CMP times. From Fig. 15 (a), it can be seen that the measured surface roughness was Ra 55 nm, because when the anodic oxidation rate of the wafer surface was higher than the MRR of the CMP process, the polishing process mainly consisted of the polishing of the SiO₂ layer by CeO₂ abrasive, and there may be oxide residues; that is, the modified layer was not completely removed. The polished surface becomes an under-polished surface. In Fig. 15 (b), the processed surface was 251 nm, and obvious pits and scratches were formed. This could possibly be because when the CMP rate was higher than the surface anodization rate, only a certain oxidation reaction occurred on the wafer surface, and the oxide layer was still very thin. Since the hardness of the SiO₂ oxide layer is lower than that of CeO₂ abrasive, the protrusions on the oxide surface were quickly removed during polishing, and then CeO₂ abrasive particles left scratches on the polished surface, which led to an over-polished surface. In Fig. 15 (c), the measured surface roughness was Ra 1.06 nm, which indicates that the oxidation rate was close to the polishing rate, and the generated oxide layer was simultaneously removed; thus the polished surface transformed to a just-polished surface.



(a) SWLI image after 3 min of anodizing and 5 min of CMP (Sz: 682 nm, Sa: 56.3 nm)



(b) SWLI image after 5 min of anodizing and 3 min of CMP (Sz: 1530 nm, Sa: 271 nm)



(c) SWLI image after 5 min of anodizing and 5 min of CMP (Sz: 97.6 nm, Sa: 15.1 nm)

Figure 15. SWLI images of the SiC surfaces after different processing conditions.

From the SWLI images shown in Fig. 15, both the under-polished and just-polished surface had a better surface quality than that of the over-polished surface. However, under-polishing resulted in some of the modified layer remaining on the SiC surface, and in the case of over-polishing, a rough surface with many etching pits was produced. To obtain a good surface roughness, the time must be controlled during the CMP process to result in a just-polished process.

4. CONCLUSIONS

To polish SiC without scratches or subsurface damage, a novel polishing approach, namely AOMP, that combines surface modification and mechanical polishing was proposed herein. The anodic oxidation mechanism of the SiC during AOMP was studied and an oxidation thickness model was developed for the purpose of obtaining an improved surface polishing quality and polishing efficiency. To summarize, the following conclusions are obtained from this study:

(1) During the AOMP process, the surface of the SiC wafer was oxidized and formed a soft modified layer mainly composed of SiO₂, and the hardness of the modified surface greatly decreased to 1/9 that of the as-received surface.

(2) An anodic oxidation process model based on the inner-outer double-directional diffusion theory was proposed. During the oxidation process, a transition layer containing silicon oxycarbide (Si-C-O) was formed between the SiO₂ and SiC, and protrusions and cracks were formed due to the expansion force produced by the subsurface oxidation.

(3) In accordance with the Deal-Grove model, the relationship between the oxide layer thickness and oxidation time during the SiC anodic oxidation process was described. At the initial stage of oxidation, the oxidation was promoted continuously with increasing oxidation time because of the porous structure of the oxide layer.

(4) The surface roughness after CMP indicated that a just-polished surface with good surface quality can be obtained when the anodic plasma oxidation rate matches the CMP rate.

ACKNOWLEDGEMENTS

The research is financially supported by the National Natural Science Foundation of China (No. 51575442) and the Natural Science Foundation of Shaanxi Province (No. 2016JZ011).

References

1. C.R. Eddy, Jr., D.K. Gaskill, *Science*, 324 (2009) 1398.
2. W. Qian, S. M., *J. Electrochem Soc.*, 142 (1995) 4290.
3. J.R. Grim, M. Benamara, M. Skowronski, W.J. Everson, V.D. Heydemann, *Semicond. Sci. Technol.*, 21 (2006) 1709.
4. F. Owman, C. Hallin, P. Mårtensson, E. Janzén, *J. Cryst. Growth*, 167(1996): 391.
5. H. Aida, T. Doi, H. Takeda, H. Katakura, S.W. Kim, K. Koyama, T. Yamazaki, M. Uneda, *Curr. Appl. Phys.*, 12 (2012) S41.
6. R.T. Bondokov, T. Lashkov, T.S. Sudarshan, *Jpn. J. Appl. Phys.*, 43 (2004) 43.
7. H. Deng, K. Yamamura, *CIRP Annals*, 62 (2013) 575.
8. H. Deng, M. Ueda, K. Yamamura, *Int. J. Adv. Manuf. Technol.*, 72 (2012) 1.
9. H. Deng, K. Endo, K. Yamamura, *Int J Mach Tool Manu.*, 115 (2017) 38.
10. D.H. van Dorp, J.J.H.B. Sattler, J.H. den Otter, J.J. Kelly, *Electrochimica Acta*, 54 (2009) 6269.
11. H. Deng, K. Hosoya, Y. Imanishi, K. Endo, K. Yamamura, *Electrochem. Commun.*, 52 (2015) 5.
12. T. Kurita, K. Miyake, K. Kawata, K. Ashida, T. Kato, *J. Micro Nano-Manuf.*, 5 (2017) 031004.
13. J. Murata, K. Yodogawa, K. Ban, *Int J Mach Tool Manu*, 114 (2017) 1.
14. O. Minami, R. Ito, K. Hosoo, M. Ochi, Y. Sano, K. Kawai, K. Yamamura, K. Arima, *J. Appl. Phys.*, 126 (2019) 065301.
15. W.J. Zhai, Q. Zhai, *Journal of Harbin Institute of Technology*, 51 (2019) 16.
16. K. Bourenane, A. Keffous, M. Kechouache, G. Nezzal, A. Boukezzata, T. Kerdja, *Surf. Interface Anal.*, 40 (2008) 763.
17. J. Li, X.F. Chen, D.Y. Ma, S. Jiang, X.X. Li, L. Wang, J. Dong, X.B. Hu, X.G. Xu, J.Y. Wang, M.H. Jiang, *Journal of Functional Materials*, 1 (2006) 70.
18. K. Imamura, T. Akai, H. Kobayashi, *Mater. Res. Express*, 6 (2019) 055906.
19. M. Gar Alalm, A. Tawfik, S. Ookawara, *J. Water Process. Eng.*, 8 (2015) 55.
20. N. Murakami, S. Kawakami, T. Tsubota, T. Ohno, *J. Mol. Catal. A-Chem.*, 358 (2012) 106.
21. Y. Gan, F. Zhang, *Chinese Sci. Bull.*, 61 (2016) 3930.

22. A.M. Alfantazi, T.M. Ahmed, D. Tromans, *Mater. Des.*, 30 (2009) 2425.
23. K. Yamamura, T. Takiguchi, M. Ueda, H. Deng, A.N. Hattori, N. Zettsu, *CIRP Annals*, 60 (2011) 571.
24. B.E. Deal, A.S. Grove, *J. Appl. Phys.*, 36 (1965) 3770.
25. Y. Song, S. Dhar, L.C. Feldman, G. Chung, J.R. Williams, *J. Appl. Phys.*, 95 (2004) 4953.
26. A.M. Balint, R. Szabo, L. Nánai, S. Iovan, S. Balint, *Nonlinear Studies*, 14 (2007) 7.
27. H. Deng, K. Endo, K. Yamamura, *Appl. Phys. Lett.*, 103 (2013) 111603.
28. A. Gomes, *Acta Cryst.*, 23 (1967) 610.
29. G.W.C. Kaye, T.H. Laby, Longman, (1995) London, UK.
30. S. Tanuma, C.J. Powell, D.R. Penn, *Surf. Interface Anal.*, 17 (1991) 927.
31. X. Li, A. Ermakov, V. Amarasinghe, E. Garfunkel, T. Gustafsson, L.C. Feldman, *Appl. Phys. Lett.*, 110 (2017) 141604.
32. G.L. Jiang, X.M. Shen, J. Tang, X.N. Zhang, X.P. Zhang, K. Yamamura, *Int. J. Electrochem. Sc.*, 11 (2016) 1512.

© 2020 The Authors. Published by ESG (www.electrochemsci.org). This article is an open access article distributed under the terms and conditions of the Creative Commons Attribution license (<http://creativecommons.org/licenses/by/4.0/>).